Supplementary Information

Melanin-like nanofibers with highly ordered structures achieve ultrahigh specific electromagnetic interference shielding efficiency

Peng Chen[1], Shibo He[1], Tianyou Wang[1], Chencan Wang[1], Junru Tao[1], Yiwen Li[1,]*

[1]College of Polymer Science and Engineering, State Key Laboratory of Advanced Polymer Materials, Sichuan University, Chengdu 610065, China.

E-mail: ywli@scu.edu.cn (Y.L.), Tel: +86 028-85401066

Note S1

Scanning electron microscopy (SEM) images showed the morphologies of resulting PDAs (Figure S3). It was observed that the PDAs with indole and 5,6-dihydroxyl indole retained the morphology of nanoparticles, while the PDAs with 5-hydroxylindole showed the morphology of nanofibers, which indicated the possibility of oriented assembly behavior. By controlling the ratio of 5-hydroxyindole, the length-diameter ratio of PDA nanofibers decreased with the increase of indole content, but no fiber was formed when the input was less than 0.05 mass ratio(Figure S4). Meanwhile, by controlling the ratio of 5-hydroxyindole to dopamine and the amount of alkali, the morphology of the PDA nanofibers showed regular changes, and the length-diameter ratio of the PDA nanofibers was larger with larger amount of alkali and smaller proportion and the length varied from several microns to over 100 microns at 5-hydroxyindole additive concentrations of 0.1 with 0.017 vol% ammonia liquor(Figure S5).

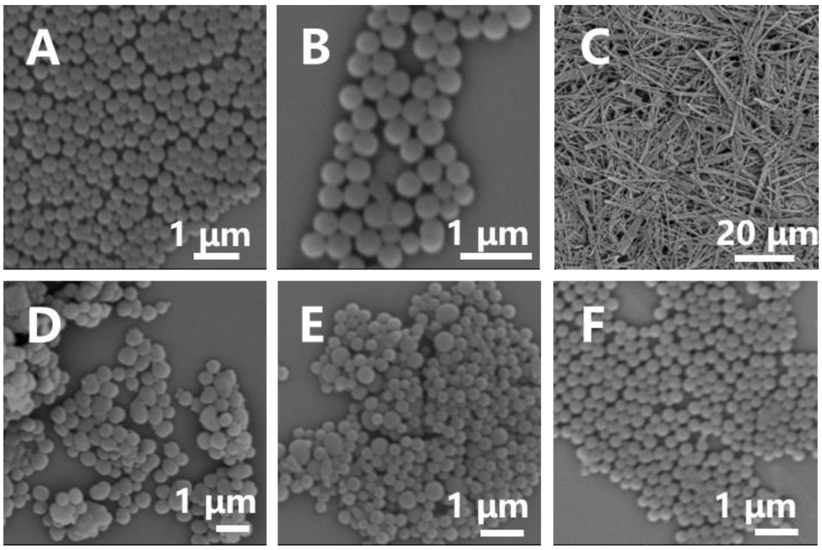

Figure S1. SEM image of PDA (A) nanoparticles, (B) nanoparticles with indole (C) nanofibers with 5-hydroxyindole (D)nanoparticles with 4-hydroxyindole (E) nanoparticls with 6-hydroxyindole and (F) nanoparticles with 5,6-Dihydroxyindole in the same method.

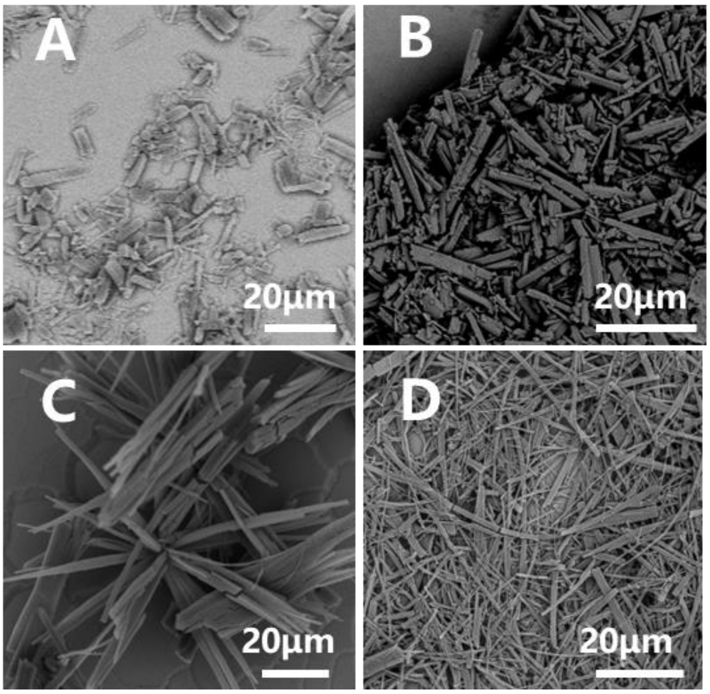

Figure S2. SEM image of nanofibers with different ratios of dopamione:5-hydroxyindole (A)1:1, (B)3:1, (C) 6:1 and (D) 9:1.

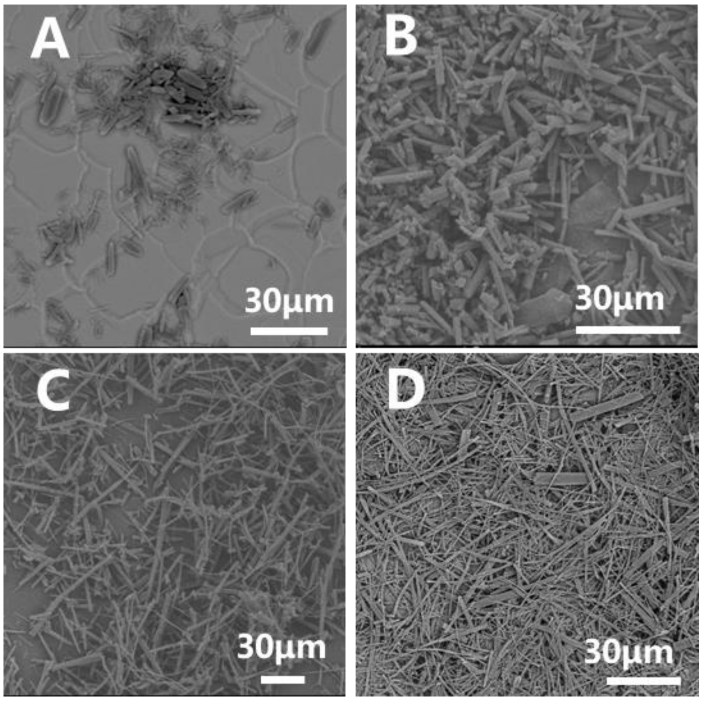

Figure S3. SEM image of nanofibers with different concentrations of ammonia liquor.

(A) 0.083 vol% (B) 0.068 vol% (C)0.034 vol% (D) 0.017 vol%.

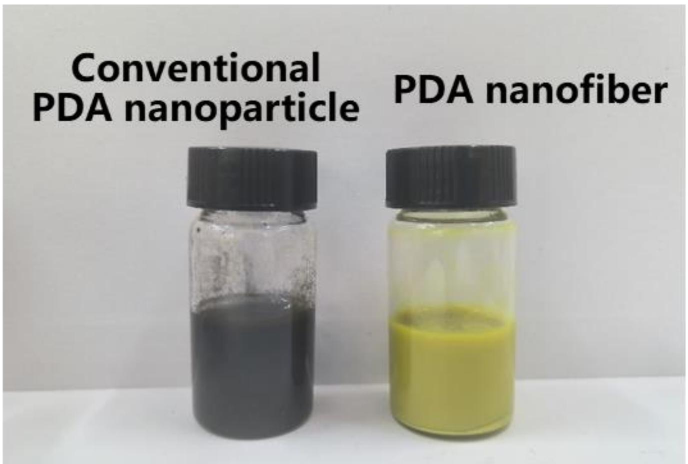

Figure S4. Optical photographs of PDA nanoparticles and nanofibers.

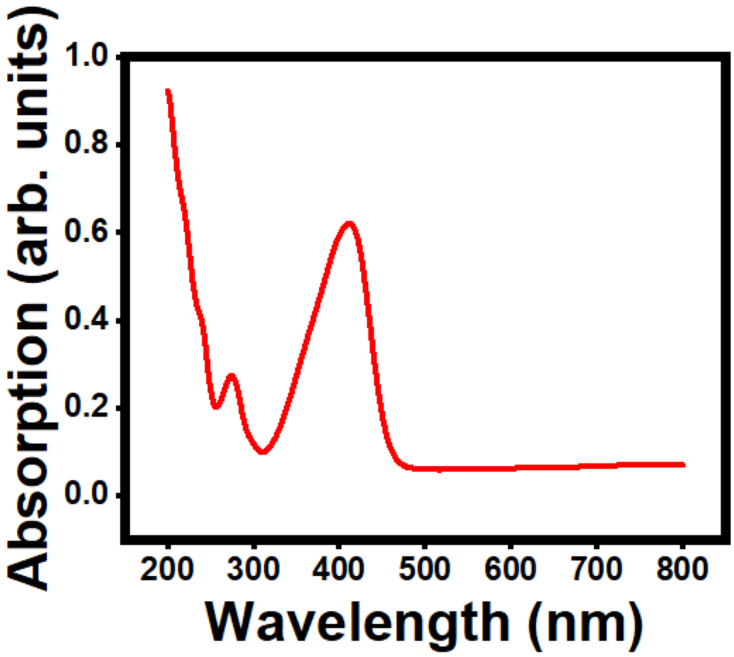

Figure S5. UV–Vis spectrum of the PDA nanofibers.

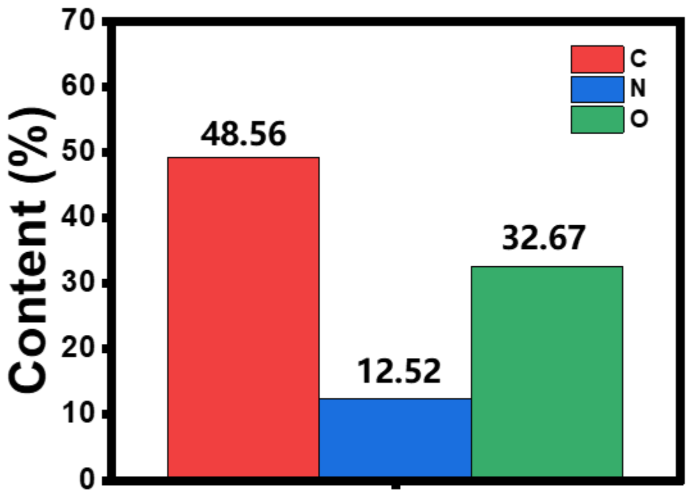

Figure S6. C, N, O element ratio of PDA nanofibers by element analyzer.

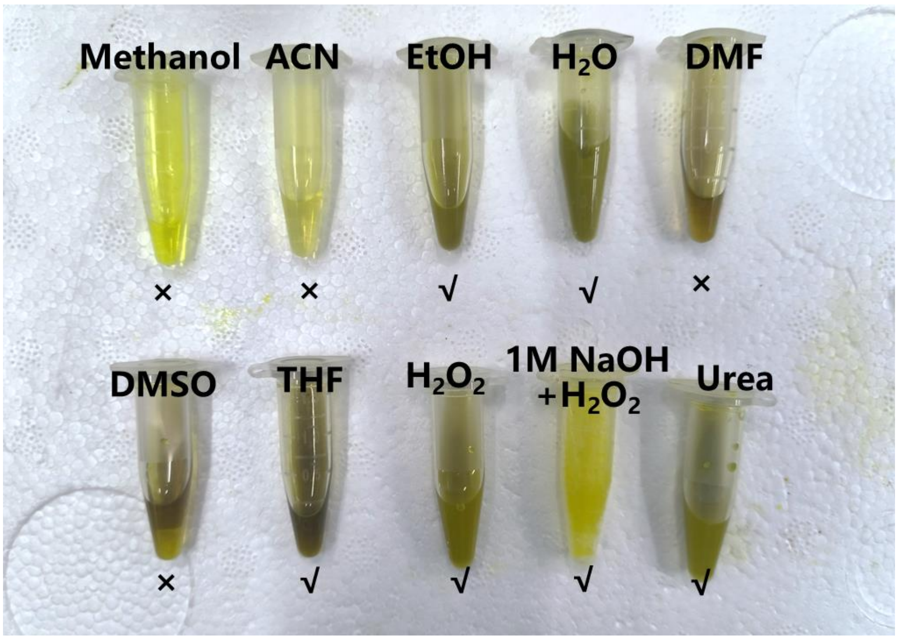

Figure S7. (a) Optical photograph of PDA nanofibers in different solvents. " √ " stands for stability, while "×" stands for degradation.

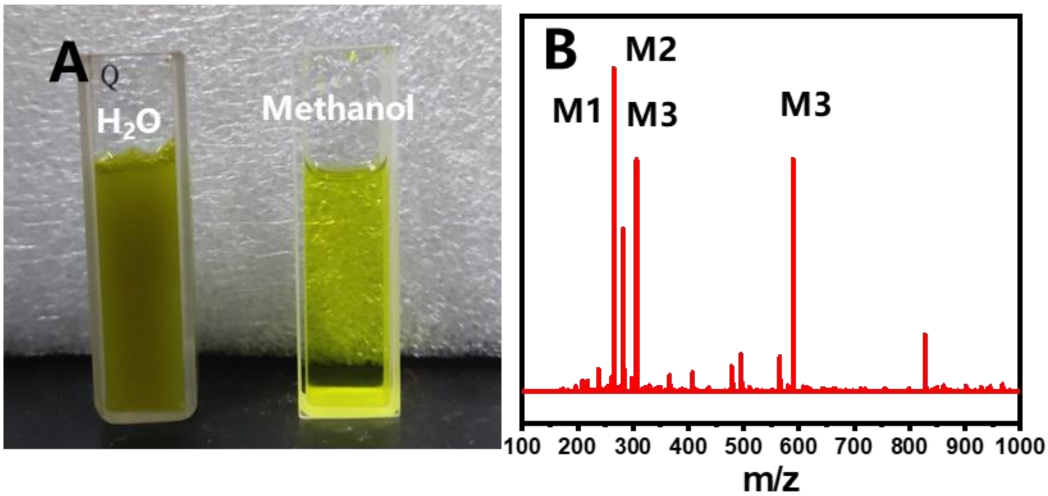

Figure S8. (A) Optical photograph of PDA nanofibers in methanol solution and water solution. (B) Electrospray Ionization Mass Spectrometry of nanofibers methanol solution.

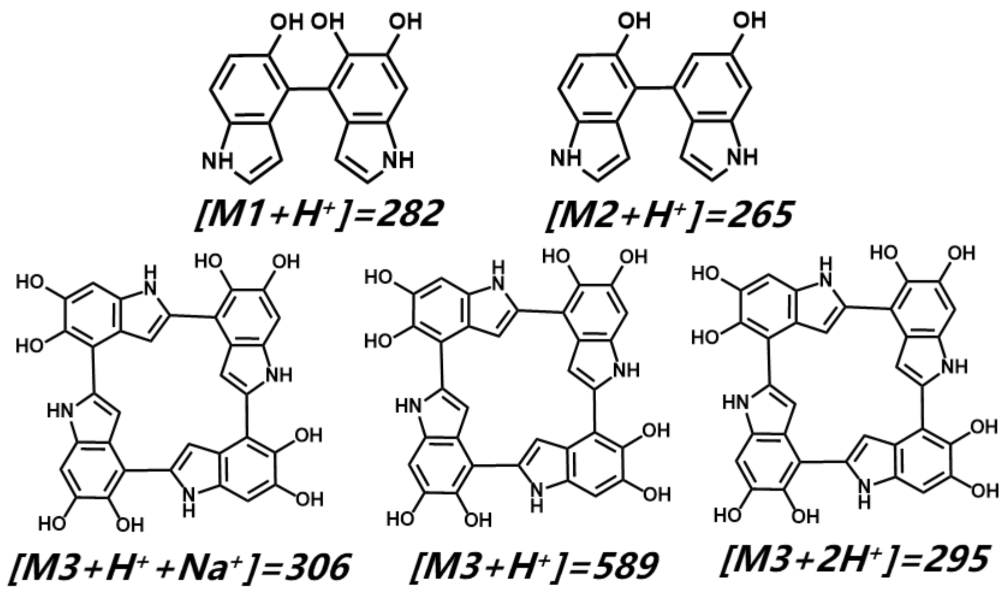

Figure S9. Proposed intermediate molecular structures assigned to main peaks in Fig. S8 and Figure 1F.

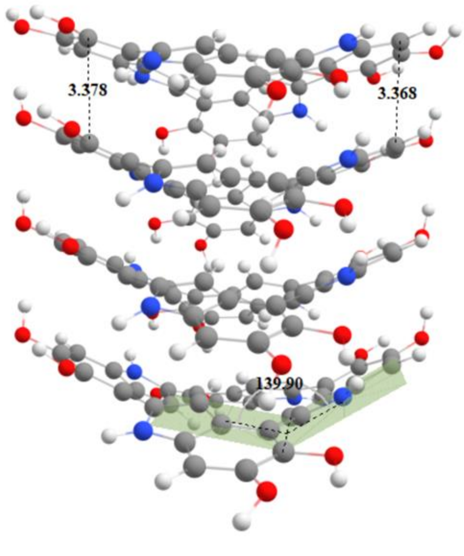

Figure S10. Tetramer structure optimized by Gaussian.

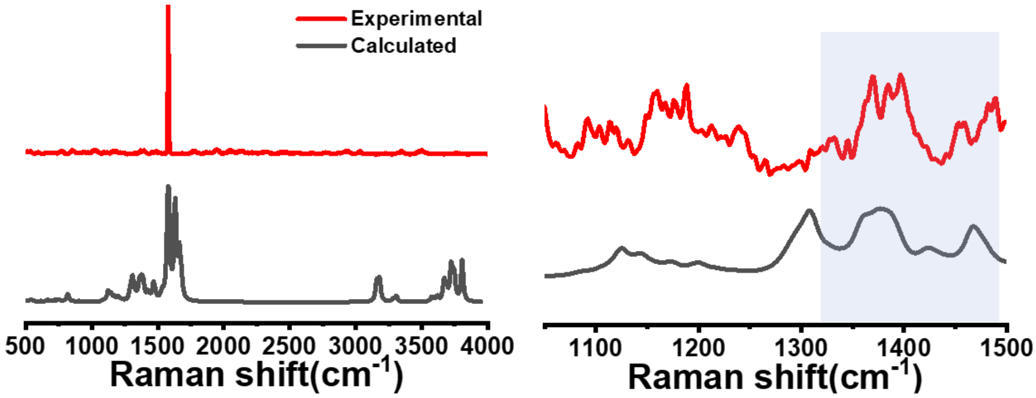

Figure S11. The calculated and experimental Raman spectra of PDA nanofibers.

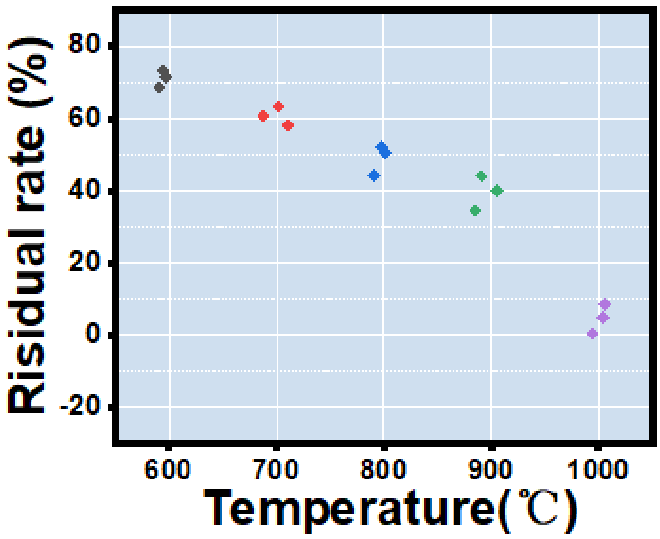

Figure S12. Residual rate of NFAGs at different temperatures.

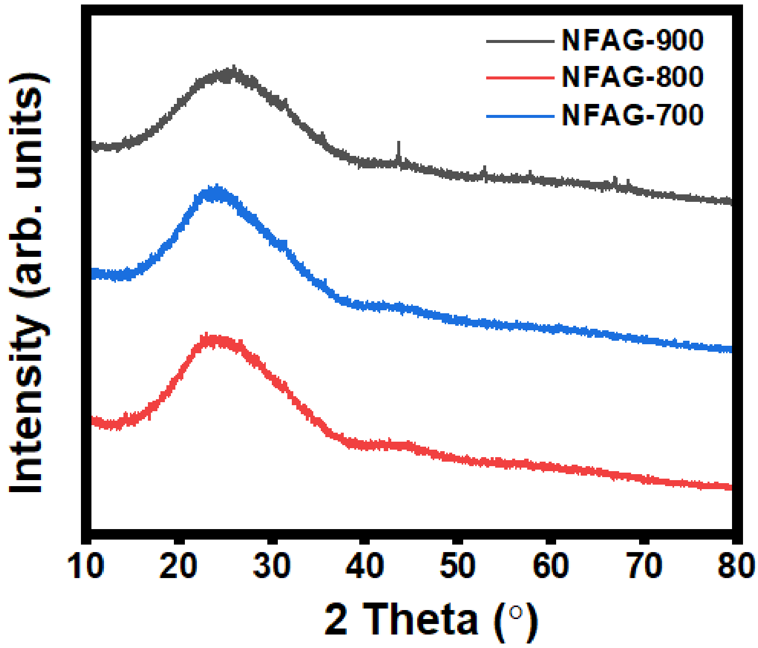

Figure S13. XRD patterns of NFAG-700, NFAG-800, NFAG-900.

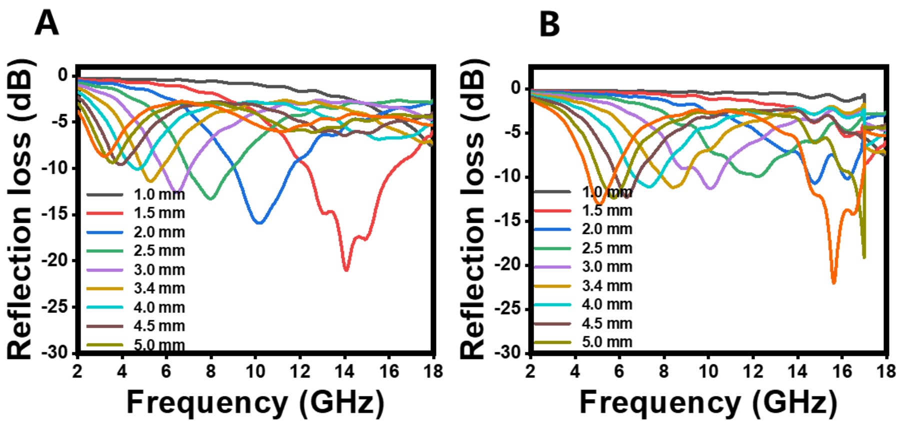

Figure S14. RL values of NFAG-900 with (A) 90% paraffin wax, (B) 70% paraffin wax.

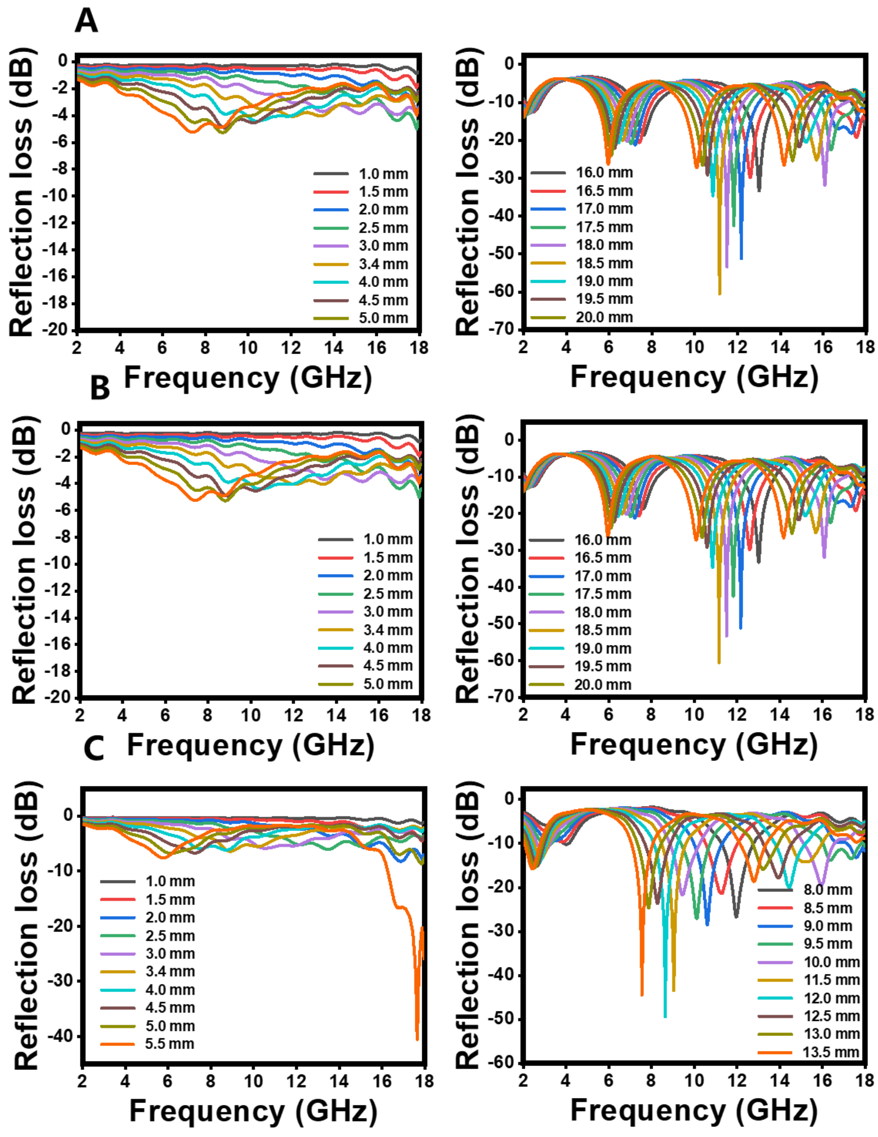

Figure S15. RL values of (A)NFAG-600, (B)NFAG-700, (C)NFAG-800 with 20%

paraffin wax.

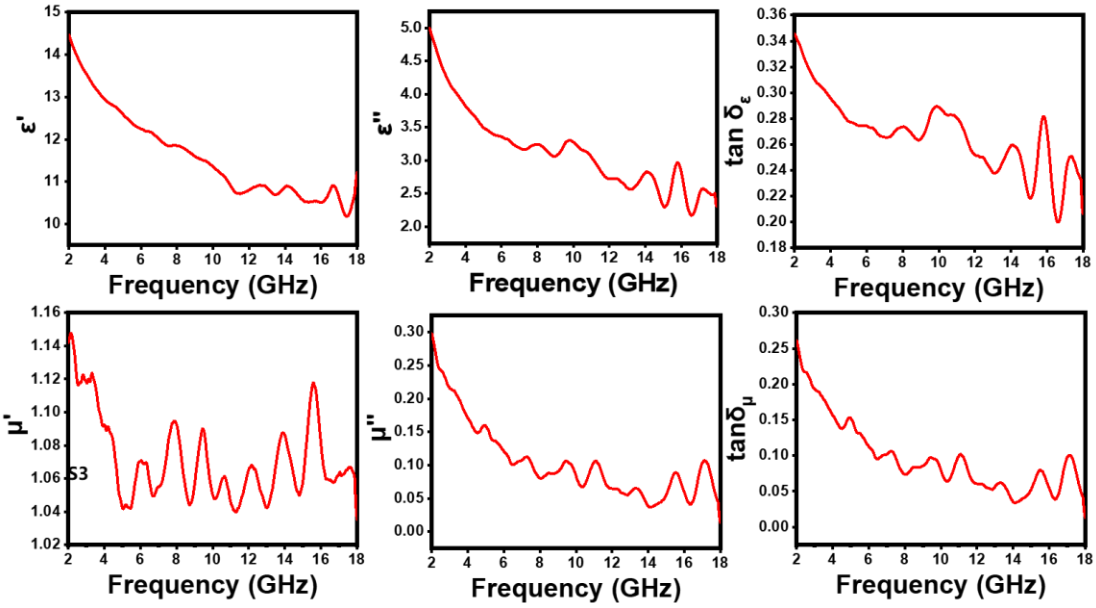

Figure S16. The relevant electromagnetic parameters of NFAG-900.

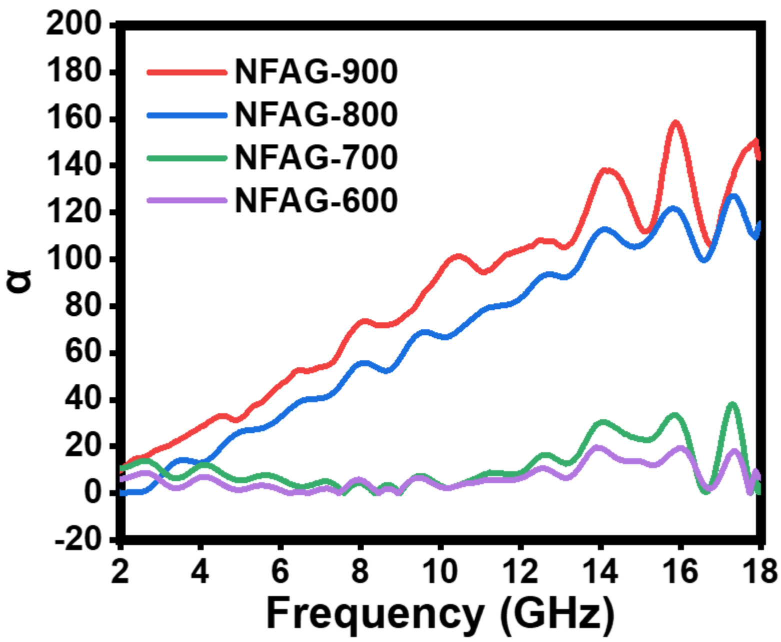

Figure S17. The attenuation constant of NFAGs.

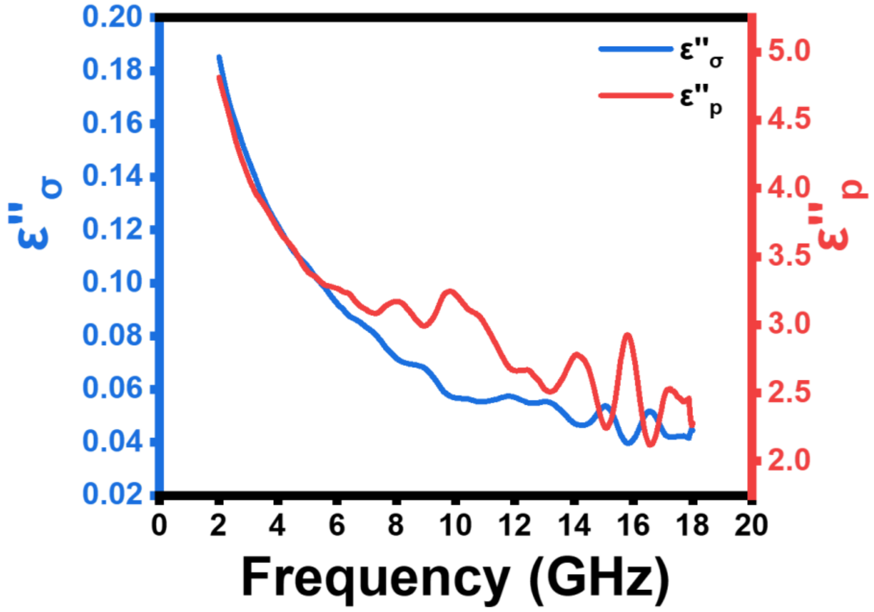

Figure S18. Fitted electromagnetic parameters of NFAG-900.

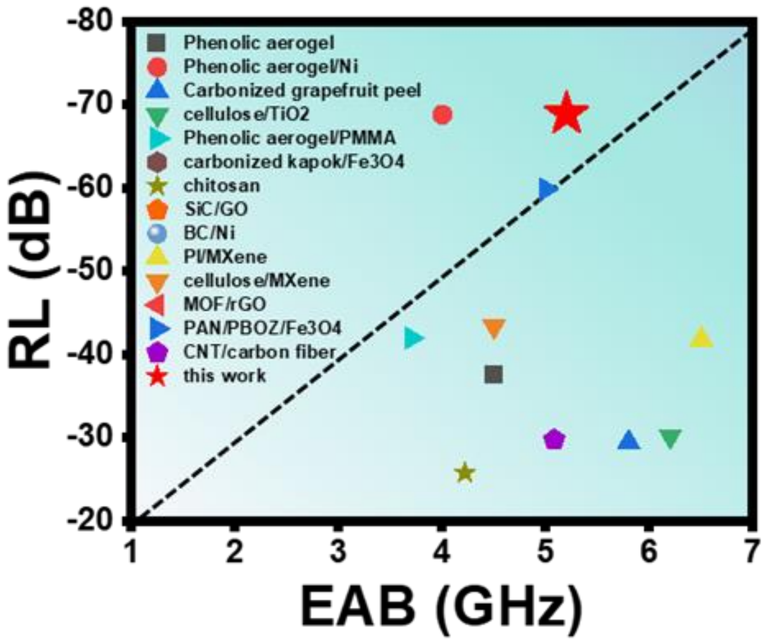

Figure S19. Comparison of RL and EAB of typical reported carbon aerogels for more related work.

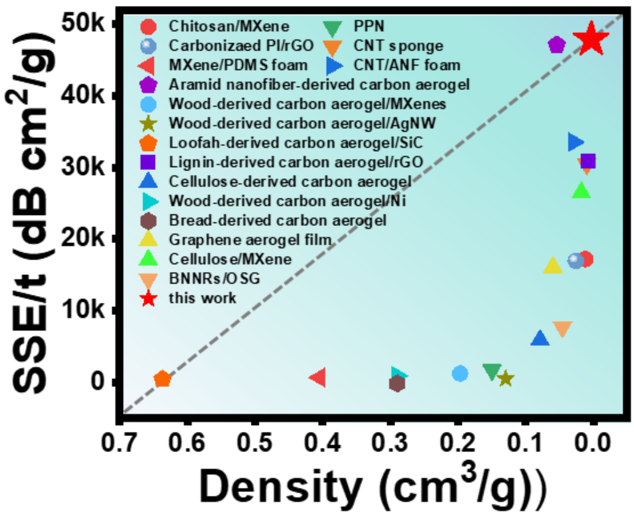

Figure S20. Comparison of SSE/t of typical reported carbon aerogels as a function of density for more related work.

Table S1. Comparison of RL and EAB of typical reported carbon aerogels.

Materials	RL (dB)	EAB (GHz)	Reference
Phenolic aerogel	**-37.5**	4.5	[1]
Phenolic aerogel/Ni	-68.8	4	[2]
Carbonized grapefruit peel	-29.5	5.8	[3]
cellulose/TiO_2	-30.2	6.2	[4]
Phenolic aerogel/PMMA	-42	3.7	[5]
carbonized kapok/Fe_3O_4	-17.3	2.1	[6]
chitosan	-25.8	4.22	[7]

SiC/GO	−47.3	4.7	[8]
BC/Ni	−55.5	5.35	[9]
PI/MXene	-41.8	6.5	[10]
cellulose/MXene	-43.4	4.5	[11]
MOF/rGO	− 58.1	6.48	[12]
PAN/PBOZ/Fe_3O_4	-59.85	5	[13]
CNT/carbon fiber	29.8	5.08	[14]
This work	**-68.9**	**5.25**	

Table S2. Comparison of SSE/t of typical reported carbon aerogels as a function of density.

Materials	**SSE/t (dB cm^2/g)**	**Density (cm^3/g)**	**Reference**
Chitosan/MXene	17184	0.0119	[15]
PPN	1700	0.15	[16]
Wood-derived carbon aerogel/Ni	882.9	0.29	[17]
Bread-derived carbon	-180.5	0.29	[18]

aerogel			
Wood-derived carbon aerogel/AgNW	465.1	0.13	19
Loofah-derived carbon aerogel/SiC	421.4	0.637	20
Carbonizaed PI/rGO	16938.8	0.026	21
Cellulose-derived carbon aerogel	5892.4	0.079	22
Graphene aerogel film	16071.4	0.06	23
CNT sponge	30444.4	0.01	24
MXene/PDMS foam	665.4	0.405	25
CNT/ANF foam	33528.3	0.029	26
Aramid nanofiber-derived carbon aerogel	47122.6	0.0544	27
Lignin-derived carbon aerogel/rGO	30750	0.008	28
Wood-derived carbon aerogel/MXenes	1206	0.197	29

Cellulose/MXene	26500	0.018	30
BNNRs/OSG	7700	0.0458	31
This work	**40785.9**	**0.00311**	

References:

1. Wang, K.J., Ye, Z.W., Li, X.Q. & Yang, J.N. Nanoporous resorcinol-formaldehyde based carbon aerogel for lightweight and tunable microwave absorption. *Mater Chem Phys* **278**, 125718 (2022).
2. Zhao, H.B. *et al.* Magnetic and Conductive Ni/Carbon Aerogels toward High-Performance Microwave Absorption. *Industrial & Engineering Chemistry Research* **57**, 202-211 (2018).
3. Gu, W.H. *et al.* Environmentally Friendly and Multifunctional Shaddock Peel-Based Carbon Aerogel for Thermal-Insulation and Microwave Absorption. *Nano-Micro Letters* **13**, 102 (2021).
4. Wang, Y.Y. *et al.* Carbon aerogel microspheres with in-situ mineralized TiO2 for efficient microwave absorption. *Nano Research* **15**, 7723-7730 (2022).
5. Mahani, A.A., Motahari, S. & Nayyeri, V. Electromagnetic and microwave absorption characteristics of PMMA composites filled with a nanoporous resorcinol formaldehyde based carbon aerogel. *RSC Advances* **8**, 10855-10864 (2018).
6. Song, S.K. *et al.* Carbon aerogel based composite phase change material derived from kapok fiber: Exceptional microwave absorbility and efficient solar/magnetic to thermal energy storage performance. *Composites Part B-Engineering* **226**, 109330 (2021).
7. Chen, X.T. *et al.* Morphology control of eco-friendly chitosan-derived carbon aerogels for efficient microwave absorption at thin thickness and thermal stealth. *Green Chemistry* **24**, 5280-5290 (2022).
8. Jiang, Y., Chen, Y., Liu, Y.J. & Sui, G.X. Lightweight spongy bone-like graphene@SiC aerogel composites for high-performance microwave absorption. *Chemical Engineering Journal* **337**, 522-531 (2018).
9. Liang, L.L. *et al.* Ultralight, flexible carbon hybrid aerogels from bacterial cellulose for strong microwave absorption. *Carbon* **162**, 283-291 (2020).

10. Dai, Y., Wu, X.Y., Liu, Z.S., Zhang, H.B. & Yu, Z.Z. Highly sensitive, robust and anisotropic MXene aerogels for efficient broadband microwave absorption. *Composites Part B-Engineering* **200**, 108263 (2020).
11. Jiang, Y. *et al.* Hierarchically structured cellulose aerogels with interconnected MXene networks and their enhanced microwave absorption properties. *Journal of Materials Chemistry C* **6**, 8679-8687 (2018).
12. Huang, X.G. *et al.* Ultralight Magnetic and Dielectric Aerogels Achieved by Metal-Organic Framework Initiated Gelation of Graphene Oxide for Enhanced Microwave Absorption. *Nano-Micro Letters* **14**, 107 (2022).
13. Li, Y. *et al.* Multifunctional Organic-Inorganic Hybrid Aerogel for Self-Cleaning, Heat-Insulating, and Highly Efficient Microwave Absorbing Material. *Advanced Functional Materials* **29**, 201807624 (2019).
14. Cheng, Y. *et al.* Lightweight and Flexible Cotton Aerogel Composites for Electromagnetic Absorption and Shielding Applications. *Advanced Electronic Materials* **6**, 201900796 (2020).
15. Wu, S.Q. *et al.* Ultralight and hydrophobic MXene/chitosan-derived hybrid carbon aerogel with hierarchical pore structure for durable electromagnetic interference shielding and thermal insulation. *Chemical Engineering Journal* **446**, 137093 (2022).
16. Zhang, L.Y. *et al.* Phthalonitrile-Based Carbon Foam with High Specific Mechanical Strength and Superior Electromagnetic Interference Shielding Performance. *ACS Applied Materials & Interfaces* **8**, 7422-7430 (2016).
17. Zheng, Y. *et al.* Lightweight and Hydrophobic Three-Dimensional Wood-Derived Anisotropic Magnetic Porous Carbon for Highly Efficient Electromagnetic Interference Shielding. *ACS Applied Materials & Interfaces* **12**, 40802-40814 (2020).
18. Yuan, Y. *et al.* Multifunctional Stiff Carbon Foam Derived from Bread. *ACS Applied Materials & Interfaces* **8**, 16852-16861 (2016).
19. Yuan, Y. *et al.* Stiff, Thermally Stable and Highly Anisotropic Wood-Derived Carbon Composite Monoliths for Electromagnetic Interference Shielding. *ACS Applied Materials & Interfaces* **9**, 21371-21381 (2017).
20. Li, S.T., Liu, D.Y., Li, W.C. & Sui, G.X. Strong and Heat-Resistant SiC-Coated Carbonized Natural Loofah Sponge for Electromagnetic Interference Shielding. *ACS Sustainable Chemistry & Engineering* **8**, 435-444 (2020).
21. Liu, J. *et al.* Superelastic and multifunctional graphene-based aerogels by interfacial reinforcement with graphitized carbon at high temperatures. *Carbon* **132**, 95-103 (2018).
22. Zhou, Z.H. *et al.* Structuring dense three-dimensional sheet-like skeleton networks in biomass-derived carbon aerogels for efficient electromagnetic interference shielding. *Carbon* **152**, 316-324 (2019).
23. Xi, J.B. *et al.* Graphene aerogel films with expansion enhancement effect of high-performance electromagnetic interference shielding. *Carbon* **135**, 44-51 (2018).

24. Lu, D.W. *et al.* Flexible, lightweight carbon nanotube sponges and composites for high-performance electromagnetic interference shielding. *Carbon* **133**, 457-463 (2018).
25. Wu, X.Y. *et al.* Compressible, durable and conductive polydimethylsiloxane-coated MXene foams for high-performance electromagnetic interference shielding. *Chemical Engineering Journal* **381**, 122622 (2020).
26. Hu, P.Y. *et al.* Multifunctional Aramid Nanofiber/Carbon Nanotube Hybrid Aerogel Films. *ACS Nano* **14**, 688-697 (2020).
27. Yao, J.R. *et al.* Ultrathin Self-Assembly MXene@flake Carbonyl Iron Composites with Efficient Microwave Absorption at Elevated Temperatures. *Advanced Electronic Materials* **7**, 202100587 (2021).
28. Zeng, Z.H. *et al.* Ultralight and Highly Elastic Graphene/Lignin-Derived Carbon Nanocomposite Aerogels with Ultrahigh Electromagnetic Interference Shielding Performance. *ACS Applied Materials & Interfaces* **10**, 8205-8213 (2018).
29. Liang, C.B. *et al.* Ultra-light MXene aerogel/wood-derived porous carbon composites with wall-like "mortar/brick" structures for electromagnetic interference shielding. *Science Bulletin* **65**, 616-622 (2020).
30. Wu, N. *et al.* Ultrathin Cellulose Nanofiber Assisted Ambient-Pressure-Dried, Ultralight, Mechanically Robust, Multifunctional MXene Aerogels. *Advanced Materials* **35**, 202207969 (2022).
31. Feng, L. *et al.* Superelastic, Highly Conductive, Superhydrophobic, and Powerful Electromagnetic Shielding Hybrid Aerogels Built from Orthogonal Graphene and Boron Nitride Nanoribbons. *ACS Nano* **16**, 17049-17061 (2022).